drones

MDPI

Article

Sensitivity Analysis of Unmanned Aerial Vehicle Composite Wing Structural Model Regarding Material Properties and Laminate Configuration

Artur Kierzkowski [1], Jakub Wróbel [1,*], Maciej Milewski [1] and Angelos Filippatos [2]

[1] Department of Technical Systems Operation and Maintenance, Faculty of Mechanical Engineering, Wroclaw University of Science and Technology, 50-372 Wroclaw, Poland; artur.kierzkowski@pwr.edu.pl (A.K.); maciej.milewski@pwr.edu.pl (M.M.)
[2] Department of Mechanical Engineering and Aeronautics, University of Patras, 26504 Patras, Greece; angelos.filippatos@upatras.gr
* Correspondence: jakub.wrobel@pwr.edu.pl

Abstract: This study optimizes the structural design of a composite wing shell by minimizing mass and maximizing the first natural frequency. The analysis focuses on the effects of polyvinyl chloride (PVC) foam thickness and the fiber orientation angle of the inner carbon layers, with the outer layers fixed at ±45° for torsional rigidity. A Multi-Objective Genetic Algorithm (MOGA), well suited for complex engineering problems, was employed alongside Design of Experiments to develop a precise response surface model, achieving predictive errors of 0% for mass and 2.99% for frequency. The optimal configuration—90° and 0° fiber orientations for the upper and lower layers and a foam thickness of 1.05 mm—yielded a mass of 412 g and a frequency of 122.95 Hz. These findings demonstrate the efficacy of MOGA in achieving innovative lightweight aerospace designs, striking a balance between material efficiency and structural performance.

Keywords: unmanned aerial vehicle (UAV); composite structures; Design of Experiment; response surface methodology; vibration

Academic Editor: Mostafa Hassanalian

Received: 12 December 2024
Revised: 20 January 2025
Accepted: 25 January 2025
Published: 28 January 2025

Citation: Kierzkowski, A.; Wróbel, J.; Milewski, M.; Filippatos, A. Sensitivity Analysis of Unmanned Aerial Vehicle Composite Wing Structural Model Regarding Material Properties and Laminate Configuration. *Drones* **2025**, *9*, 99. https://doi.org/10.3390/drones9020099

1. Introduction

The advent of composite materials has revolutionized modern aviation, providing a sophisticated alternative to traditional metallic structures. These advanced materials, characterized by their heterogeneous composition and exceptional mechanical properties, have become indispensable in the design and manufacturing of aircraft [1]. Composite materials, typically consisting of a polymer matrix reinforced with fibers such as carbon, glass, or aramid, provide a unique combination of high strength-to-weight ratios, corrosion resistance, and design flexibility [2]. These attributes are crucial for meeting the stringent requirements of performance, safety, and efficiency in modern aeronautical engineering.

1.1. State of the Art

In the realm of unmanned aerial vehicles (UAVs), composite materials are indispensable for meeting stringent design requirements and overcoming critical performance challenges. These materials are particularly valued for their lightweight and robust properties, which enhance the structural efficiency of UAVs. The use of composites has further intensified due to the sector's demand for lightweight, robust, and highly maneuverable platforms [3]. UAVs, which encompass applications ranging from reconnaissance and

surveillance to commercial deliveries and environmental monitoring [4–8], benefit significantly from the reduced structural weight afforded by composites. By reducing the structural mass, composite materials not only enhance payload capacity and fuel efficiency but also improve the operational range and endurance of UAVs—parameters that are critical for both military and civilian applications.

However, the advantages of composite materials are accompanied by distinct challenges, particularly in dynamic performance. Composite structures, unlike metallic structures, exhibit orthotropic and heterogeneous properties, leading to unique vibrational behavior. This makes their vibrational response highly complex and sensitive to factors such as fiber orientation, matrix composition, and layer stacking sequence [9]. Modal analysis, focusing on natural frequencies and vibration modes, is crucial for evaluating and improving the dynamic performance of advanced material structures [10,11].

In contemporary aviation, significant emphasis is placed on the development of high-aspect-ratio wings to reduce induced drag and improve aerodynamic performance. Concurrently, significant efforts are directed toward minimizing the structural mass of these components. However, the combination of high aspect ratios and reduced weight introduces challenges related to substantial structural deformations, particularly at the wingtips [12]. Moreover, the resulting structures are susceptible to nonlinear dynamic behaviors, which are inherently challenging to analyze and may cause undesirable aeroelastic phenomena such as limit cycle oscillations [13] or structural failure under specific conditions [14].

To mitigate these issues, it is imperative to limit deformations by increasing the structural stiffness of the wings, thereby preventing adverse aeroelastic phenomena such as flutter or divergence [15]. An increase in stiffness directly influences the natural frequencies of the wing structure. Consequently, the design process prioritizes elevating these natural frequencies to enhance dynamic stability and prevent destructive aeroelastic interactions [16]. Thus, the attainment of higher natural frequencies constitutes a pivotal objective in the design of modern wing structures, ensuring both structural integrity and operational reliability under dynamic loading conditions.

1.2. Outlook and Scope of the Investigation

The primary scope of this study was to conduct a sensitivity analysis using Design of Experiments (DoE) approach combined with a Response Surface Model (RSM) based on a numerically verified and experimentally validated model of a UAV's composite wing. The research aims to address critical challenges in UAV wing design, such as vibration behavior, weight reduction, and stiffness optimization. These challenges are directly linked to the need for an effective balance between structural performance and dynamic behavior.

To optimize the wing structure, the study focused on maximizing stiffness—quantified through the maximization of the first natural frequency—while minimizing mass to meet the weight efficiency goals that are essential in the aerospace sector. Sensitivity analysis plays a crucial role in identifying the most influential design variables and their interactions, allowing for a comprehensive understanding of how different factors affect the overall performance.

The use of RSM allows for the exploration of nonlinear relationships between design variables and structural responses, providing a robust framework for evaluating the performance of different configurations. This approach represents a novel application of these techniques in tailoring UAV structures, providing a robust framework for achieving optimal design solutions amidst competing objectives.

2. Materials and Methods

2.1. Design of a Study Case

The object of the analysis is the wing of a UAV (Figure 1) designed for the SAE Aero Design 2022 competition, which fully complies with the competition's regulatory requirements [17]. The aircraft is 2.47 m long, with a wingspan of 3.05 m and an empty weight of 4.5 kg. The wing's aspect ratio is 6.6. The wing was fabricated using a hand lay-up process combined with vacuum-bagging technology. The hand lay-up and vacuum-bagging processes are sufficiently repeatable for this application due to its simplicity and established methodology. Although minor variations may occur due to manual handling, the process consistently achieves the required material properties and structural performance.

Figure 1. The studied UAV.

The wing shell is made of two layers of carbon fiber fabric, specifically Aspro spread tow carbon fabric A-80 in an epoxy resin matrix, oriented at ±45° with respect to the chord of the wing, with a 1.2 mm sheet of foamed PVC sandwiched between them (Figure 2). Both the upper and lower skins of the shell were fabricated in this manner. The shell's upper and lower skins were both manufactured using this sequence.

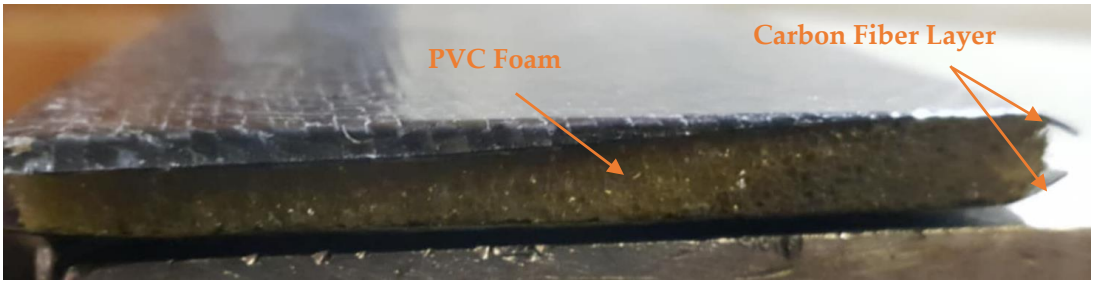

Figure 2. Laminate layer sequence.

Figure 3 illustrates the structure of the UAV wing, which consists of a spar, three ribs, two stringers, a wing pipe, a wing pipe sleeve, and a bolt. The wing pipe and bolt connect the wings to the fuselage. The wing pipe is made of carbon fiber with a diameter of 22 mm and a thickness of 1 mm. The wing pipe sleeve is also fabricated of wound carbon fiber. The remaining components are fabricated from 5 mm thick PVC foam. In the semi-shell structure, the shell primarily carries torsional loads, making it crucial to ensure adequate torsional stiffness. To achieve this, the carbon fiber layers were arranged at a ±45°, a configuration that effectively enhances the shell's ability to carry twisting forces.

This strategic fiber orientation is essential for maintaining the structural integrity and performance of the wing under operational conditions. The internal structure is optimized to carry bending loads.

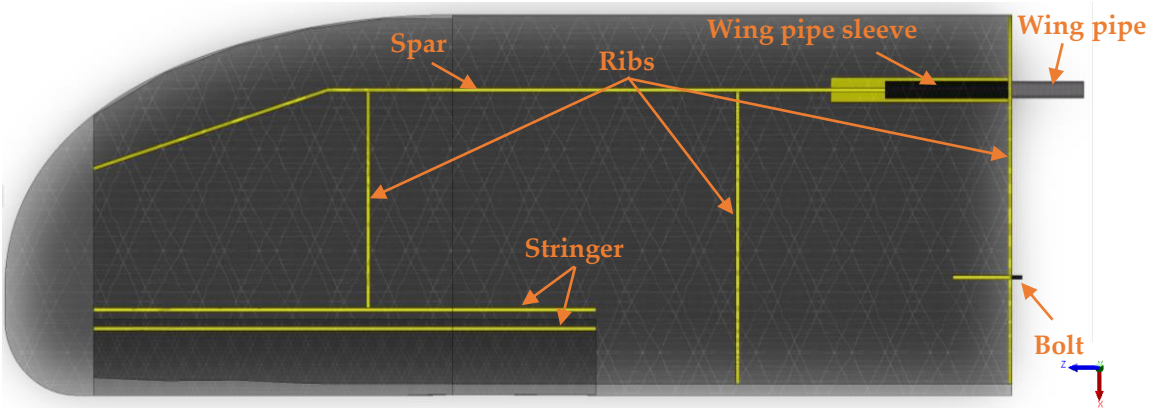

Figure 3. Internal elements of the UAV wing—spar, ribs, stringer, bolt, wing pipe sleeve, and wing pipe.

2.2. Experimental Modal Analysis of Wing

Modal analysis is a key tool for evaluating the dynamic properties of structures such as the mentioned UAV wing. These properties define the structure's behavior under excitation conditions. In a modal analysis, the dynamic control equation can be represented as follows:

$$\boldsymbol{M}\ddot{\boldsymbol{x}} + \boldsymbol{C}\dot{\boldsymbol{x}} + \boldsymbol{K}\boldsymbol{x} = \boldsymbol{F}(t), \tag{1}$$

where

$\boldsymbol{M}$ represents the mass matrix.
$\boldsymbol{C}$ represents the damping matrix.
$\boldsymbol{K}$ represents the stiffness matrix.
x represents the displacement vector.
$\dot{x}$ represents the velocity vector.
$\ddot{x}$ represents the acceleration vector.
$F(t)$ represents the vector of external loads applied to the structure.
If case of damping and external loads are neglected, the equation becomes the following:

$$\boldsymbol{M}\ddot{\boldsymbol{x}} + \boldsymbol{K}\boldsymbol{x} = 0, \tag{2}$$

When simple harmonic motion occurs, the equation is as follows:

$$\left(\boldsymbol{K} - \boldsymbol{\omega_i}^2\boldsymbol{M}\right)\boldsymbol{\varphi_i} = 0, \tag{3}$$

where

$\boldsymbol{\omega_i}$ represents the i-th mode natural frequency of the structure.
$\boldsymbol{\varphi_i}$ represents the i-th mode shape of the structure.

To incorporate the specific mechanical properties of the composite material into the stiffness matrix, it is necessary to apply the Classical Lamination Theory (CLT). CLT provides a framework for analyzing laminated composite structures by considering their orthotropic and heterogeneous characteristics. Through this methodology, the effective stiffness properties of the composite are determined by aggregating the contributions of individual lamina, each characterized by its unique material constants and orientation. For a single lamina, assuming a plane stress condition whose principal axes coincide with

the principal axes of the reference coordinate system, the stiffness matrix is represented as follows:

$$[\boldsymbol{Q}] = \begin{bmatrix} Q_{11} & Q_{12} & 0 \\ Q_{12} & Q_{22} & 0 \\ 0 & 0 & Q_{66} \end{bmatrix}, \tag{4}$$

$$Q_{11} = \frac{E_1}{1 - v_{12}v_{21}}, \tag{5}$$

$$Q_{22} = \frac{E_2}{1 - v_{12}v_{21}}, \tag{6}$$

$$Q_{12} = \frac{v_{12}E_2}{1 - v_{12}v_{21}}, \tag{7}$$

$$Q_{66} = G_{12}. \tag{8}$$

where

Q_{ij} represents reduced stiffnesses.

E_1 represents the stiffness along the longitudinal direction of the fibers.

E_2 represents stiffness transverse to the direction of fibers.

v_{12} represents the Poisson's ratio along the longitudinal direction of the fibers.

v_{21} represents the Poisson's ratio along the transverse direction of the fibers.

G_{12} represents the shear modulus.

When the orientation angles of the laminate layers differ from the principal axes of the composite structure, it becomes necessary to account for the transformations of stiffness properties between local and global coordinate systems. This adjustment ensures that the mechanical behavior of the composite is accurately represented in the context of the overall structural analysis. Such transformations involve rigorous application of tensorial mechanics and are essential for constructing the effective stiffness matrices that govern the in-plane, bending, and coupling responses of the laminate. The detailed procedures for these transformations are comprehensively discussed in several works about the mechanics of composite materials [9,18–21].

Experimental modal analysis was conducted using a flexibly suspended aircraft to emulate free-flight conditions (Figure 4). A DEWESoft DS-MS-440 440N, 0–5 kHz sine, electrodynamic shaker manufactured in Trbovlje, Slovenia, was employed for excitation due to its ability to deliver precise and repeatable signals, avoiding the potential damage associated with using a modal hammer.

System excitation was controlled with a Dytran model 5860B IEPE impedance head manufactured in Chatsworth, US consisting of a 100 mV/lbf force sensor and a 100 mV/g accelerometer within the same housing. The impedance head acceleration signal was used as a closed-loop control signal for the shaker amplifier. Structural response was measured using a PCB Piezotronics 356A03 miniature light weight triaxial piezoelectric IEPE accelerometer with 10 mV/g sensitivity, manufactured in Depew, US. The tests targeted a frequency range of 0–1100 Hz, with the excitation signal forms listed in Table 1. The sampling frequency was set to 20 kHz, and each excitation sweep lasted approximately 77 s. Measurement points were strategically distributed across the wing's upper surface (Figure 5), while responses from the aileron surface were excluded due to its distinct dynamic behavior as an active control surface. Following guidance from studies like the NASA X-56A aircraft research [22], the aileron was locked at a 0-degree deflection to prevent issues such as drooping and inconsistencies in the data, ensuring more reliable and controlled test conditions.

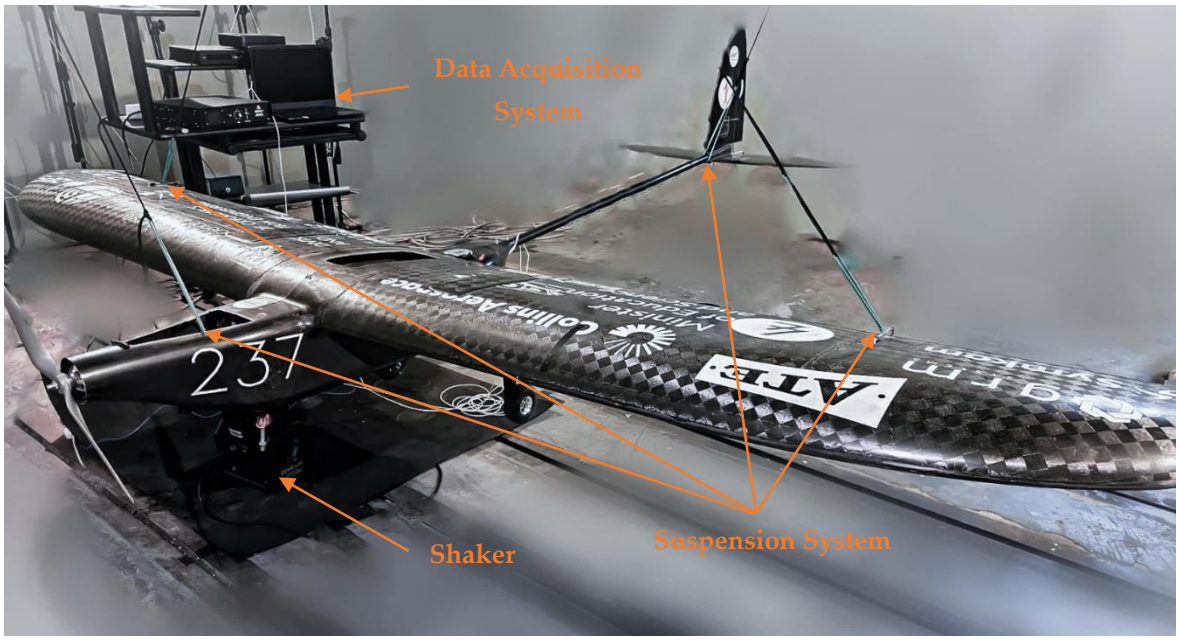

Figure 4. Experimental test configuration.

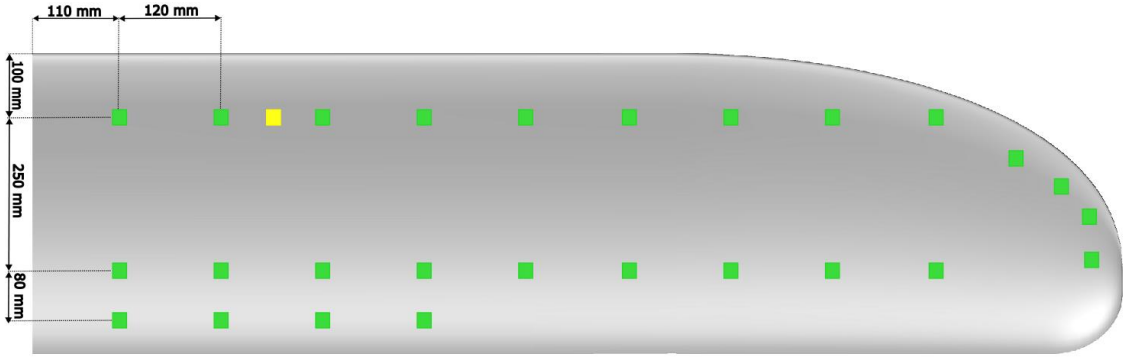

Figure 5. Measurement and excitation points placement on the wing. Green—measurement points; yellow—excitation point.

Table 1. Excitation signal form.

Sequence	Start Frequency [Hz]	End Frequency [Hz]	Start Acceleration [g]	End Acceleration [g]	Sweep Rate [Hz/s]
1	5	70	0.1	1.5	10
2	70	100	1.5	2.1	8
3	100	300	2.1	3.3	12
4	300	500	3.3	5.0	10
5	500	1100	5.0	2.6	20

2.3. Numerical Modal Analysis of Wing

The Finite Element Method (FEM) is a widely adopted approach for analyzing the dynamic behavior of composite materials. Its strength lies in its ability to accurately represent the orthotropic and heterogeneous properties of such materials. FEM allows researchers to predict essential dynamic characteristics such as natural frequencies, mode shapes, and stress distributions under various loading conditions. However, the accuracy of these predictions heavily depends on the appropriate selection of input parameters and

careful model calibration. FEM models often overestimate structural stiffness, highlighting the critical role of experimental validation in ensuring reliable results. Friswell and Mottershead [23] emphasized the importance of incorporating experimental data to refine FEM models and improve simulation fidelity. Recent studies have increasingly focused on combining experimental insights with FEM to achieve a more accurate characterization of dynamic properties. For instance, Lin, Yang, Bai, and Qin [24] conducted both numerical and experimental modal analyses of the nose landing gear to investigate its dynamic properties and validate the accuracy of the computational models. The simulations were performed using ANSYS Workbench, enabling detailed insights into the natural frequencies and mode shapes of the structure. To complement the numerical analysis, an experimental study was conducted using a modal hammer, which allowed for precise measurements of the gear's response to dynamic excitation. This combined approach ensured a robust evaluation of the landing gear's behavior under operational conditions and highlighted the importance of integrating experimental data for improving the reliability of FEM predictions. Qaumi and Hashemi [25] validated FEM models for composite rocket components by conducting experimental modal analysis. Their approach involved pairing numerical simulations in Ansys with hammer tap tests, utilizing laser vibrometers for precise measurements.

This study included a comprehensive modal analysis of a UAV wing, encompassing both numerical simulations and experimental validation. The simulations were conducted using Ansys Composite Prep/Post (ACP), an advanced module tailored for modeling and optimizing composite structures. The ACP module allows for precise definition of material properties and layer configurations, including variations in fiber orientation, material composition, and thickness for each layer. A key feature is its ability to simulate complex layer sequences, essential for modeling fiber orientations, that significantly affect simulation accuracy. The simulation was conducted under free-free boundary conditions to replicate the wing's unconstrained behavior during flight [26,27]. This setup ensured accurate calculation of natural frequencies and mode shapes without imposing artificial constraints [28]. The wing was modeled as a shell part with upper and lower skins, reflecting the actual manufacturing process. The layer sequence in the model replicated the physical wing's configuration, enhancing its accuracy.

Owing to the inability to perform material tests on the actual material used in the wing structure, the material properties were assigned from the software's library (*Epoxy Carbon Woven (230 GPa) Wet)*. The upper skin's carbon fiber layer orientation is shown in Figure 6.

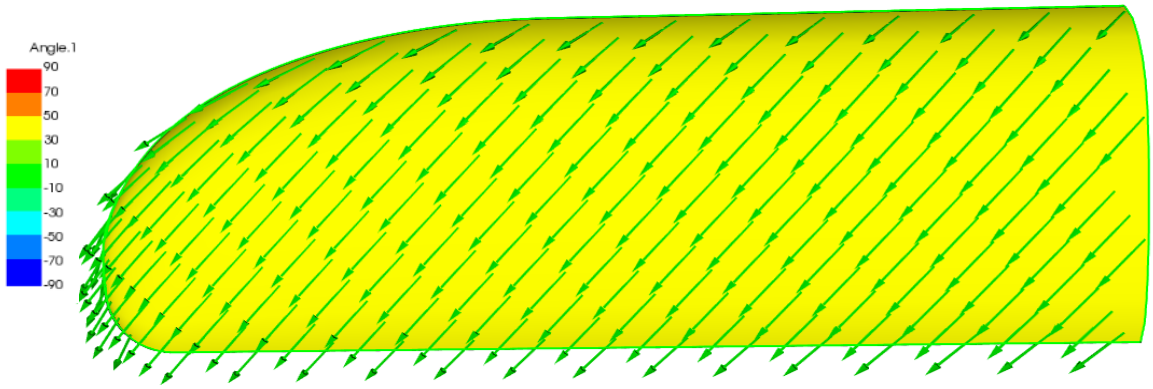

Figure 6. Carbon fiber layer orientation on upper skin of the wing.

To ensure a detailed and realistic representation, the finite element model included all internal structural components illustrated in Figure 3, guaranteeing that the simulation reflected the actual configuration of the wing. The aileron was modeled as an integral part

of the wing in the model. Determining the natural frequencies of vibration and conducting aeroelastic analyses of control surfaces are distinct topics in aviation, studied in dedicated research due to the complexity of the problem and the distinct behavior of these surfaces compared to the rest of the aircraft wing. Mesh sizes were meticulously selected to balance precision and computational efficiency, with detailed meshing for critical components such as bolts, ribs, and stringers. A mesh size of 10 mm was used for the wing shell, employing the Shell 181 element type presented in Figure 7. Volumetric elements were meshed using a hexahedral mesh: 2.5 mm for ribs and stringers, 1 mm for bolts, and 5 mm for the spar. The simulation model assumed the structure to be continuous, regular, and smooth.

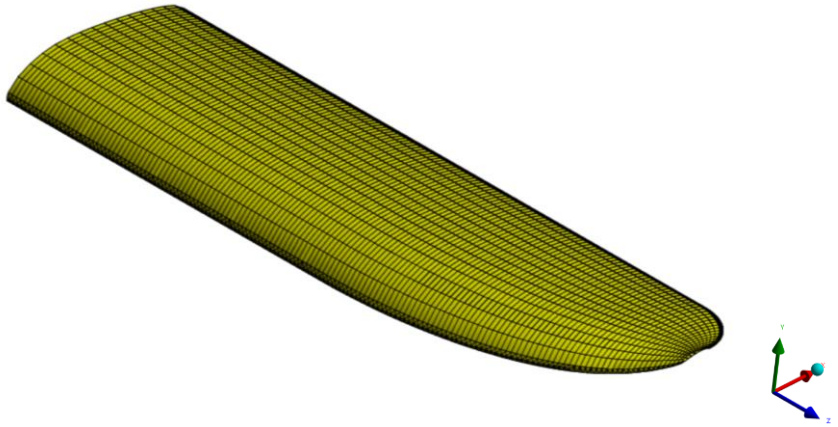

Figure 7. Finite element mesh on the wing.

2.4. Design of Experiment and Response Surface Methodology

Design of Experiments (DoE) is a methodology that facilitates systematic planning and analysis of experiments to efficiently study processes or systems. In computational simulations, DoE allows for the exploration of a model's behavior without the need for physical experiments. This approach enables rapid assessment of the impact of key input parameters on the results and facilitates design optimization.

DoE involves running a limited number of simulations at carefully selected points within the design space. From these simulations, a mathematical model—known as a Response Surface—was developed to predict outcomes for any parameter combination within the defined range. This process enables the identification of the most influential variables, their impact on the results, and the examination of interactions and nonlinear relationships, all without extensive simulations.

DoE offers significant time and computational resource savings while providing comprehensive insights into the behavior of the system under study. This approach is particularly valuable in complex engineering projects, where optimization is critical and the cost of running numerous simulations must be minimized.

Response Surface Methodology (RSM), introduced by Box and Wilson [29], utilizes a series of experimental trials to identify an optimal response influenced by various factors. It serves as a mathematical and statistical tool for optimizing processes by assessing the relationship between input variables (factors) and output results (responses) [30]. A key advantage of RSM is its ability to generate reliable outcomes with fewer experiments, as the response surface can be developed by fitting the results from a limited set of trial data points.

The process of RSM begins with defining the response parameters of the experiment. Next, the relevant input parameters for the experiments must be determined. The mean response is an unknown function that depends on the selected parameters [31]. The goal of RSM is to determine this mean response, which forms the response surface when plotted. To

do so, a set of experiments is conducted based on a predefined model. The results presented below were obtained using the Ansys Workbench Response Surface Optimization module, which support various types of DoE, including the following:

- Central Composite design;
- Optimal Space-Filling design;
- Box–Behnken design;
- Sparse Grid Initialization;
- Latin Hypercube Sampling design.

Optimizing the stiffness and mass of a composite structure with varying fiber orientation is inherently a nonlinear problem. The change in fiber orientation does not result in a linear change in stiffness or natural frequency. As the fiber angle changes, the material's mechanical response—such as its modulus of elasticity, shear strength, and ultimately its vibration frequencies—varies nonlinearly due to complex interaction between composite layers and their response to applied loads and deformations.

In this case, Sparse Grid Initialization was selected as the most suitable method for the analyzed problem due to its effectiveness in handling the nonlinear relationships between design variables and responses as well as its computational efficiency in high-dimensional design spaces [32].

In the context of such a nonlinear problem, traditional linear optimization methods may not be sufficient to capture the true behavior of the system—the composite UAV wing. Sparse Grid methods are especially useful for efficiently sampling design spaces without requiring exhaustive evaluations. The Sparse Grid design is a special discretization technique, which can be traced back to the Smolyak algorithm [33]. It is based on hierarchical basis, a representation of a discrete function space, which is equivalent to the conventional nodal basis, and a sparse tensor product construction [32]. When the Design of Experiments type is set to Sparse Grid Initialization in Ansys, the adaptive model operates based on the user-specified level of accuracy. This method enhances the accuracy of the response surface by automatically refining the design matrix in areas where the relative error in the output parameters is more significant. Sparse Grid Initialization uses a Clenshaw–Curtis Grid [34] with levels 0 and 1, where level 0 corresponds to the current values of the parameters, and level 1 involves two additional points per input parameter.

A key advantage of Sparse Grid Initialization is its efficiency in refining the grid only in necessary directions, reducing the number of design points required to achieve a high-quality response surface. Furthermore, this method is particularly effective for handling discontinuities within the model, making it highly suitable for complex, nonlinear optimization problems where changes in one parameter can lead to disproportionate effects on the response [35].

By concentrating refinement efforts on regions with significant model error, Sparse Grid Initialization provides a computationally efficient method for exploring the design space while maintaining high accuracy [35].

2.5. The Optimization Model

In preparing the experiment, the design variables were defined as described earlier: the thickness of the PVC foam layer ranged from 1 mm to 5 mm, and the fiber orientation angles of the inner carbon layers ranged from 0° to 90°, with 1° increments. These ranges were chosen to enable effective optimization by exploring a wide array of potential configurations within practical limits. The selection of these ranges was also guided by manufacturing

constraints and the expected mechanical performance of the composite material. The planned experiment adhered to the following conditions:

$$\begin{cases} 1\text{ mm} \leq T_{PVC} \leq 5\text{ mm} \\ 0^\circ \leq O_{IBH} \leq 90^\circ \\ 270^\circ \leq O_{IUH} \leq 360^\circ \\ O_{OBH} = 45^\circ = constans \\ O_{OUH} = 45^\circ = constans \\ minimaze\ M_{shell} \\ maximize\ f_1, \end{cases}$$

where T_{PVC} represents the foam thickness; O_{IBH} is orientation of the inner layer of the lower skin; O_{IUH} is orientation of the inner layer of the upper skin, O_{OBH}, O_{OUH} are orientations of the outer layers of the lower and upper skin, respectively; M_{shell} is mass of the shell; and f_1 is the first natural frequency value [Hz].

The fiber orientation of the upper skin of the wing was set at 45° relative to the X-axis and continued seamlessly onto the lower skin of the wing. This wrapping of the fiber from the upper to the lower skin ensured the continuity of the composite structure. However, due to the chosen coordinate system, to correctly represent this continuity in the simulation, the fiber angle for the lower skin was specified as 315° with respect to the X-axis. This adjustment accurately represented the continuous fiber orientation across both skins, as intended in the structure.

For the Sparse Grid Initialization, 100 design points were selected to construct the response surface. These points were chosen to efficiently cover the design space while minimizing computational effort. Model refinement was conducted adaptively, with a maximum allowed error of 5%, which offered a balance between accuracy and computational cost.

Additionally, 25 verification points were defined to validate the accuracy of the response surface model. These points were distinct from the design points, serving as an independent check on the model's predictive performance. Verification points are critical for confirming the accuracy of the response surface model, offering an additional layer of validation to ensure accurate predictions for various combinations of design variables. This process provided for a more robust basis for confidently exploring the design space during the optimization phase.

3. Results of the Wing Design

3.1. Numerical and Experimental Results Comparision

The results obtained from the experiment and simulations were compiled and compared. Table 2 presents the results for the first four natural frequencies.

Table 2. Comparison of results obtained in simulation and experiment for the first four natural frequencies.

Mode ID	Simulation [Hz]	Experiment [Hz]	Difference [%]
1st natural frequency	86.35	79.85	8.18
2nd natural frequency	125.58	114.94	9.26
3rd natural frequency	139.89	134.98	3.64
4th natural frequency	162.03	157.75	2.71

The differences between the experimental and simulation results are not negligible, ranging from 2.71% to 9.26%. This can be attributed to the simplifications made in the simulation model, which assumed continuity and homogeneity of the structure. However, a significant correlation in the mode shapes was observed as presented in Figure 8, resulting in a satisfactory representation of the dynamic behavior. Further work will focus on refining the model to reduce these discrepancies.

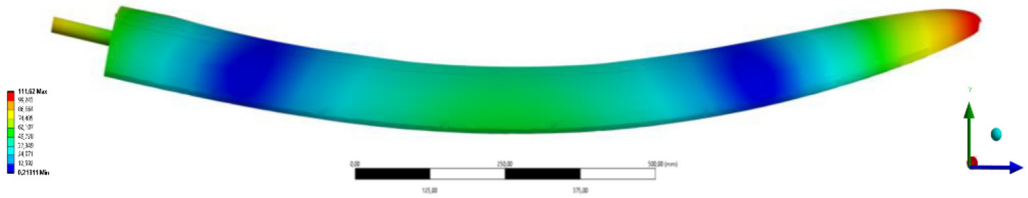

(**a**) Mode shape obtained from simulation.

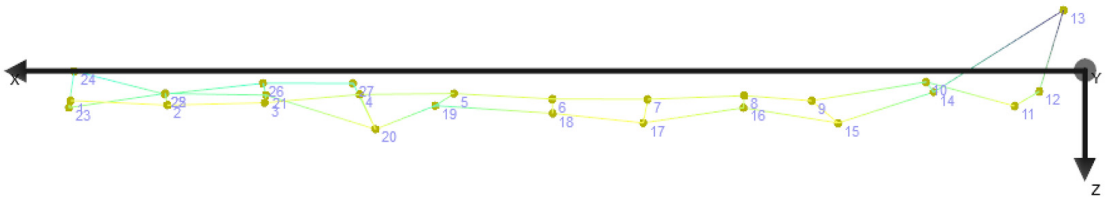

(**b**) Mode shape obtained from experiment.

Figure 8. Comparison of the 1st mode shape obtained from simulation and experiment.

3.2. Optimization of Wing Structural Performance

Comparison of simulated and experimental results confirmed the FEM model's suitability as a reliable source of information despite some deviations. Considering the aviation industry's focus on minimizing mass while maximizing stiffness and structural strength, an optimization process was initiated.

To achieve the objective of minimizing mass while maximizing stiffness by shifting the first natural frequency to higher values, the optimization process focused on two key design variables: the thickness of the PVC foam layer and the fiber orientation angle of the inner carbon layer. The variables are shown on the cross-section of the wing in Figure 9. The stiffness was evaluated based on the first natural frequency, which serves as a reliable indicator of structural rigidity. The decision to vary these specific parameters was grounded in their direct impact on both mass and stiffness.

The wing structure consists of two skins, each manufactured from a sequence of materials: carbon fiber oriented at $\pm 45°$, a PVC foam, and another carbon fiber layer at $\pm 45°$. A critical assumption is that the outer layers, oriented at $\pm 45°$, will remain unchanged. This ensures the structure's ability to effectively carry torsional stresses, as the $\pm 45°$ orientation is optimal for handling shear loads caused by torsion [34]. The placement of these layers farther from the torsion axis maximizes their contribution to torsional stiffness, which is a key functional requirement of the shell. Keeping this configuration unchanged preserves the integrity of the torsion-resisting mechanism of the wing.

The thickness of the PVC layer is selected as a variable because it directly influences both the mass and the stiffness of the structure. Increasing the core thickness enhances bending and shear stiffness but also increases mass. The inner carbon fiber orientation is varied because its angle significantly affects the in-plane stiffness and natural frequency without altering the structural capacity to resist torsion, unlike changes to the outer layers.

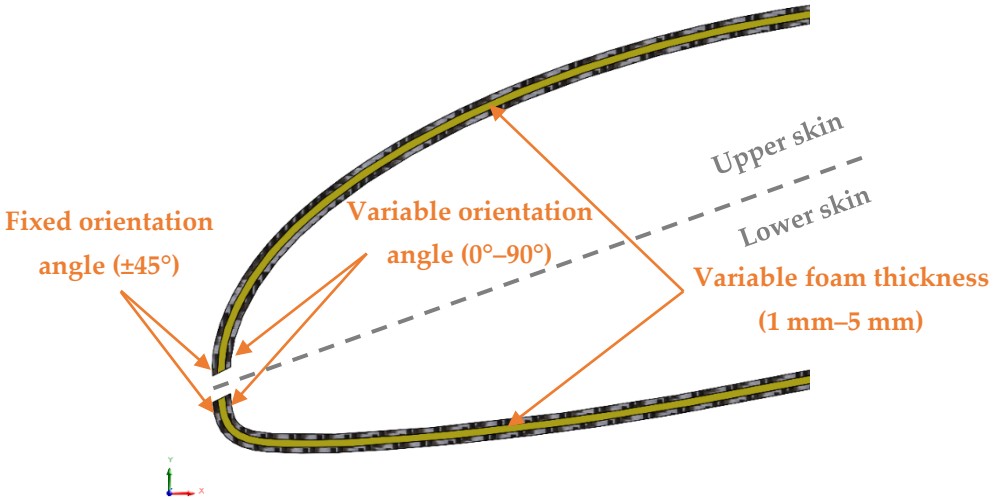

Figure 9. Cross-section of the wing with marked variables layers and fixed layers.

The selection of the range for the design variables is based on practical considerations, such as the limitations of the hand lay-up process, including the difficulty in achieving precise fiber orientations and consistent layer thickness by hand. These constraints ensure both feasibility and relevance to real-world manufacturing processes, with the design variables selected within ranges that can be reliably produced using this method.

For the fiber orientation angle of the inner carbon layers, the range was chosen from 0° to 90°, with the possibility to vary the angle in 1° increments. This range is appropriate because fiber orientations outside of this range would likely provide negligible differences in performance, making finer increments impractical and unnecessary. Moreover, in practical manufacturing, such small angle changes are difficult to achieve, so a 1° step provides a balance between computational efficiency and accuracy without unnecessarily complicating the optimization process.

For the PVC foam thickness, the range was set from 1 mm to 5 mm, as these values are typical in production and readily available from suppliers. Foam thicknesses outside of this range are not commonly used in structural applications like this, and values within this range provide a realistic spectrum of options that are commonly seen in the industry. Moreover, these thickness values are sufficient to cover the expected range of mass and stiffness variations, making them ideal for optimization purposes.

In this approach, we left the foam thickness with full flexibility within the selected bounds, meaning that the optimization could explore all possible values within the 1 mm to 5 mm range. This flexibility ensured that the optimization process could determine the most efficient thickness for the given design requirements while still staying within practical and realistic manufacturing constraints.

These assumptions and variable selections ensured a focused and scientifically grounded exploration of the design space, allowing for the development of a solution that meets the competing demands of high stiffness and low mass.

For this purpose, Design of Experiments (DoE) and Response Surface Methodology (RSM) were utilized, as they provide efficient and effective tools for exploring and identifying optimal design solutions.

3.3. Sensitivity Results from Optimization Process

The optimization experiment, utilizing the Sparse Grid Initialization method, concluded after 88 design points were sampled. This approach allowed the adaptive algorithm to refine the response surface efficiently, focusing computational resources where the most significant improvements in prediction accuracy were needed. The resulting response

surface achieved an average relative error of 0% for mass predictions and 2.99% for predictions of the first natural frequency. These results demonstrate the method's robustness in handling the nonlinear relationships inherent in the problem.

Figure 10 illustrates the relationship between fiber orientation, foam thickness, and the first reported natural frequency and mass.

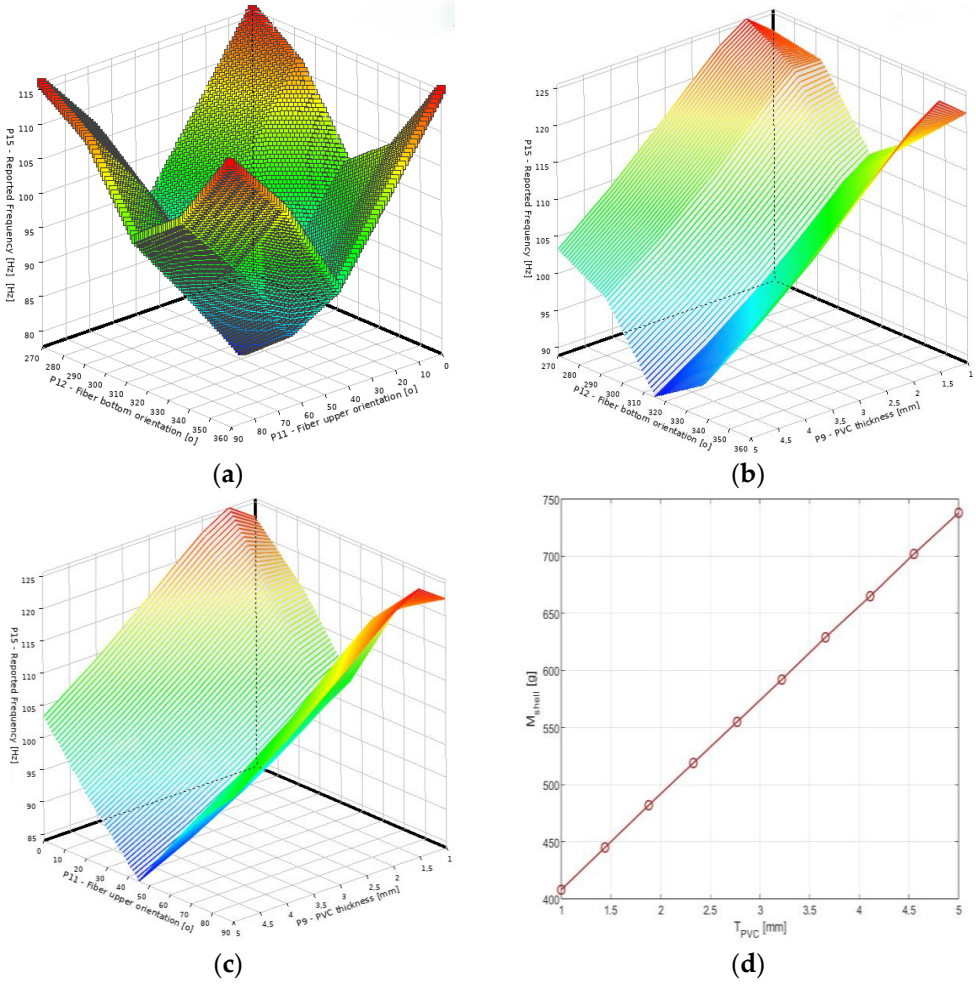

Figure 10. Relationship between orientation on fiber, foam thickness, and first reported natural frequency and mass. (**a**) Response Surface relationship between f_1 value and parameters O_{IBH} and O_{IUH}. (**b**) Response Surface relationship between f_1 value and parameters O_{IBH} and T_{PVC}. (**c**) Response Surface relationship between f_1 value and parameters O_{UBH} and T_{PVC}. (**d**) Response graph relationship between M_{shell} value and parameter T_{PVC}.

Figure 10a illustrates the relationship between the natural frequency, fiber orientation angles, and their interplay. The steep transitions visible in the graph suggest points where the dominant vibration mode shifts from bending to torsion, highlighting critical interactions between material orientation and structural dynamics. Figure 10b,c illustrate the relationship between the natural frequency, fiber orientation angles of the lower and upper skins (respectively), and the thickness of the PVC core. Figure 10d depicts the relationship between the PVC core thickness and the mass of the wing shell. This dependence is presented as a linear plot, reflecting the fact that shell mass is entirely independent of fiber orientation. The direct proportionality between PVC thickness and mass underscores the nature of this relationship, as the added material volume uniformly increases mass without any nonlinear interactions.

The configuration yielding the minimum possible mass corresponds to a PVC foam thickness of 1 mm, achieving a total shell mass of 407.95 g. This result is expected, as reducing the foam thickness directly minimizes the material volume and, consequently, the mass. In contrast, the maximum value of the first natural frequency, which is 125.58 Hz, was achieved with a foam thickness of 1.5 mm and fiber orientation angles of 90° for the upper skin and 270° for the lower skin of the wing shell. This specific combination of parameters appears to maximize the structural stiffness while remaining within the feasible range for material properties and geometric constraints.

The local sensitivity analysis revealed the relative impact of each design variable on the first natural frequency of the wing shell. The results indicate that foam thickness contributes 25.89% to the variation in frequency, while the fiber orientation of the inner layer of the upper skin accounts for 38.38%, and the fiber orientation of the inner layer of the lower skin contributes 35.73%. These values highlight that the fiber orientations play a dominant role in influencing the natural frequency, collectively accounting for over 74% of the sensitivity. The foam thickness, while less sensitive than the fiber orientations, still plays an important role in natural frequency response and carries 100% of the sensitivity of mass property of the structure. A graph chart is presented in Figure 11.

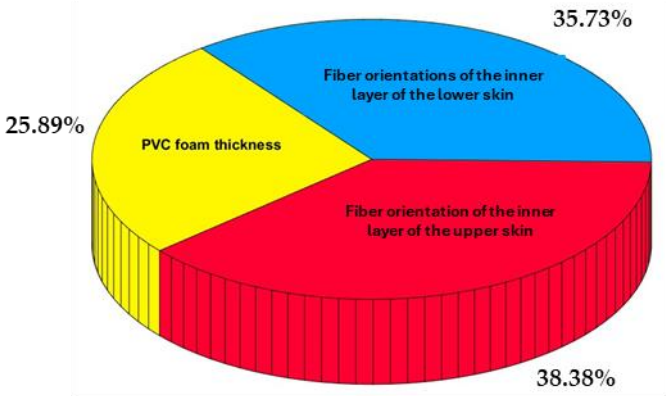

Figure 11. Sensitivity graph chart.

The optimal solution was determined using the Multi-Objective Genetic Algorithm (MOGA), an advanced variant of the widely utilized NSGA-II (Non-dominated Sorted Genetic Algorithm-II). MOGA employs controlled elitism to balance exploration and exploitation of the design space, making it particularly effective for multi-objective problems. It is designed to handle multiple objectives and constraints while striving to identify a global optimum [31].

In this case, the optimal configuration was achieved with the upper layer fiber oriented at 90°, the lower layer fiber oriented at 0°, and a PVC foam thickness of 1.05 mm. Under these parameters, the mass of the wing shell was minimized to 412 g, while the first natural frequency was maximized at 122.95 Hz. The mode shape of the proposed design is shown in Figure 12.

The mode shape corresponding to the proposed optimal point is characterized by torsional deformation.

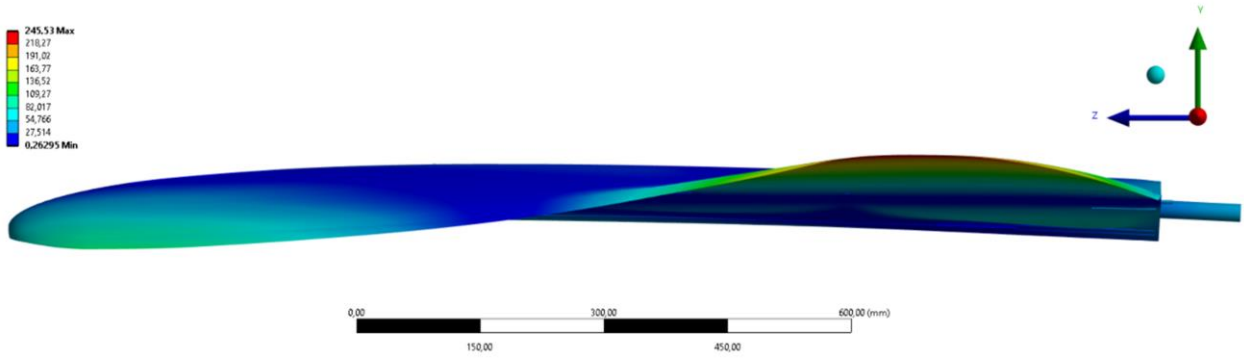

(**a**) Mode shape in YZ plane for proposed design.

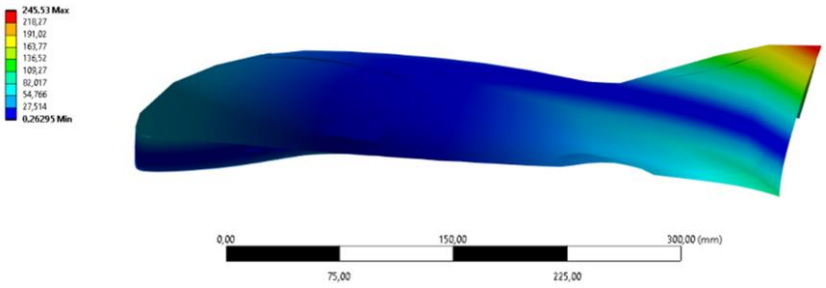

(**b**) Mode shape in XY plane for proposed design.

Figure 12. Mode shape obtained for proposed design.

4. Discussion

The Response Surface from Figure 10a provides a visualization of how the first natural frequency varies based on the fiber orientation angles of the inner carbon layers in both the upper and lower skins of the wing structure. The vertical axis represents the first natural frequency value, while the horizontal axes correspond to the fiber orientations: 0–90° for the upper skin and 270–360° for the lower skin. Notable features of the plot include distinct peaks and valleys, with sharp transitions in frequency values observed at certain points. These points of abrupt change likely indicate areas where the dominant mode of vibration shifts—from bending to torsional modes. Additionally, the surface shows regions of both gradual and rapid variation in frequency, emphasizing the sensitivity of the first natural frequency to fiber orientation. The fiber angles in the upper and lower skins interact nonlinearly, creating complex behavior across the design space. These observations highlight how fiber orientation significantly influences the dynamic properties of the composite structure, with certain configurations offering higher or lower stiffness, as inferred from the natural frequency trends. The similar contributions of fiber orientation in both the upper and lower skins are due to the balanced structural role of these layers in determining the overall bending and torsional stiffness of the wing. Further investigation is required to validate the hypothesized modal transitions observed in the sharp break points of the surface.

The relationship between PVC foam thickness and the mass of the wing shell, as depicted in Figure 10d, highlights a strictly linear dependency. This linear trend confirms that the mass of the shell is unaffected by fiber orientation, as the latter does not influence the material volume. The proportional increase in mass with thickness illustrates that the added material contributes uniformly to the overall mass, without any nonlinear effects arising from geometric or interactive parameters. Such a linear behavior is characteristic of structural systems where mass is governed solely by material density and volume.

The foam thickness influences the bending stiffness by changing the geometry of the cross-section of the wing structure. This effect reduces the sensitivity of the natural frequency to foam thickness compared to fiber orientation, which directly influences the wing's in-plane stiffness and bending stiffness. However, as the thickness of the foam increases, the inner carbon layers at 0–90° move closer to the neutral axis, which can slightly reduce the flexural stiffness of the wing. Despite this, the core material plays a role in maintaining the structural integrity and ensuring the outer layers are effectively supported, preserving the wing's strength and shape. The sensitivity analysis demonstrated that the first natural frequency of the wing shell is most strongly influenced by the fiber orientations, with the upper part's fiber orientation contributing 38.38% and the lower part's fiber orientation contributing 35.73%. The foam thickness accounts for 25.89% of the variation, indicating a secondary but still notable effect.

These findings emphasize the dominant role of fiber orientation in controlling the dynamic response of the structure. Both the upper and lower fiber orientations exhibit nearly equivalent contributions, reflecting the balanced structural significance of each layer. Conversely, the foam thickness primarily affects bending stiffness by altering the geometry of the cross-section and the position of the neutral axis, explaining its relatively lower sensitivity compared to the fibers. While the foam contributes to shear stiffness and provides structural support, the outer layers, oriented at $\pm 45^\circ$, are primarily responsible for torsional stiffness. The foam core helps in mass reduction but also plays a crucial role in maintaining the overall structural integrity. The final thickness of the core was determined by balancing bending, torsional, and shear stiffness with the need for mass minimization. Together, these parameters interact to determine the overall frequency response, illustrating the complex interplay between material and geometric factors in composite structures.

The optimal configuration identified through the MOGA method aligns with a torsional mode shape, highlighting the dynamic behavior under the specified design parameters. The fiber orientation angles are 90° (upper layer) and 0° (lower layer), coupled with the PVC core thickness of 1.05 mm. This setup enables a simultaneous mass reduction to 412 g and enhancement of structural stiffness, achieving a natural frequency of 122.95 Hz.

5. Conclusions

This study explored the optimization of a composite wing shell structure using state-of-the-art computational techniques and material configurations, emphasizing the dual objectives of minimizing mass and maximizing natural frequency. The key research design variables, such as PVC foam thickness and the fiber orientation angles of the inner carbon fiber layers, were analyzed, with the $\pm 45^\circ$ outer carbon fiber layers maintained for torsional stiffness. Optimization was performed using Design of Experiment combined with the MOGA algorithm, creating a robust numerical framework.

Response Surface Methodology revealed nonlinear relationships between design variables and structural responses, with a strong emphasis on computational efficiency. The final Sparse Grid model demonstrated a high predictive accuracy, achieving an average relative error of 0% for mass and 2.99% for the natural frequency. These results highlighted the effectiveness of Sparse Grid sampling in handling the complexities of high-dimensional design spaces, particularly for non-linear, orthotropic material behaviors.

The optimization process identified that the PVC foam thickness and fiber orientations of the upper and lower carbon layers significantly influence the structural performance. Sensitivity analysis quantified their contributions as 25.89%, 38.38%, and 35.73%, respectively. This finding underscores the intricate interplay of material distribution and orientation in achieving a high-performance design. The optimal configuration featured fiber orientations of 90° and 0° for the upper and lower layers, respectively, with a core thickness of 1.05

mm. This setup resulted in a shell mass of 412 g and a first natural frequency of 122.95 Hz, corresponding to a torsional mode shape. The selection reflects the importance of torsional stiffness in meeting aerodynamic and structural demands.

The results also highlighted key insights into the behavior of composite structures. The sharp transitions observed in the response plots indicate potential mode shape shifts, likely from bending to torsion, emphasizing the dynamic implications of fiber orientation. Furthermore, the linear dependency of shell mass on PVC core thickness validated the straightforward volumetric contribution of the core material, independent of fiber orientation or other geometric factors.

This work demonstrates the viability of advanced optimization methods, such as the MOGA algorithm and Sparse Grid Initialization, for developing lightweight and high-stiffness composite structures. By capturing the intricate relationships between material properties and performance metrics, this approach provides a scalable framework for future applications in aerospace and mechanical design. The findings not only align with theoretical predictions but also offer practical pathways for enhancing structural efficiency in composite materials.

In future work, integrating experimental validation with these computational results could refine the predictive models and address uncertainties in real-world manufacturing processes. This includes material testing as well as fabrication of a wing prototype with an optimal configuration derived from the algorithm and assessing whether the natural frequencies of this prototype align with those predicted by the RSM. The variability in material properties due to manufacturing defects as well as the potential difficulty in replicating precise fiber orientations may introduce discrepancies between simulation and experimental results.

Further exploration of dynamic mode interactions and their structural implications may also offer deeper insights into the optimization of orthotropic materials. Further symmetrical and unsymmetrical layup designs, materials, and advanced manufacturing methods should be investigated to cover the whole design–manufacturing–technologies space. This collaborative approach between computational analysis and experimental verification paves the way for designing advanced, high-performance structures that meet stringent aerospace requirements.

Author Contributions: Conceptualization, A.K., J.W., M.M., and A.F.; data curation, J.W. and M.M.; investigation, J.W. and M.M.; methodology, J.W. and A.F.; resources, A.K.; software, J.W. and M.M.; supervision, A.K.; validation, A.K., M.M., and A.F.; visualization, J.W. and M.M.; writing—original draft, J.W. and M.M.; Writing—review and editing, A.K. and A.F. All authors have read and agreed to the published version of the manuscript.

Funding: This research received no external funding.

Data Availability Statement: The data will be available on request.

Conflicts of Interest: The authors declare no conflicts of interest.

References

1. Mazlan, N.; Sapuan, S.M.; Ilyas, R.A. *Advanced Composites in Aerospace Engineering Applications*; Springer International Publishing: Cham, Switzerland, 2022. [CrossRef]
2. Yi, X.-S.; Du, S.; Zhang, L. *Composite Materials Engineering, Volume 1*; Springer: Singapore, 2018. [CrossRef]
3. Karpenko, M.; Stosiak, M.; Deptuła, A.; Urbanowicz, K.; Nugaras, J.; Królczyk, G.; Żak, K. Performance Evaluation of Extruded Polystyrene Foam for Aerospace Engineering Applications Using Frequency Analyses. *Int. J. Adv. Manuf. Technol.* **2023**, *126*, 5515–5526. [CrossRef]
4. Rufino, G.; Conte, C.; Basso, P.; Tirri, A.E.; Donato, V. Mission Design and Validation of Fixed-Wing Unmanned Aerial Vehicle for Environmental Monitoring. *Drones* **2024**, *8*, 641. [CrossRef]

5. Ahmed, M.; Rasheed, H.; Salloum, M.; Hegazy, M.; Bahrami, M.R.; Chuchkalov, M. Seal Pipeline: Enhancing Dynamic Object Detection and Tracking for Autonomous Unmanned Surface Vehicles in Maritime Environments. *Drones* **2024**, *8*, 561. [CrossRef]
6. Li, F.; Kunze, O. A Comparative Review of Air Drones (UAVs) and Delivery Bots (SUGVs) for Automated Last Mile Home Delivery. *Logistics* **2023**, *7*, 21. [CrossRef]
7. Lartey, S. The Impact of Drones on Modern Warfare and Surveillance: Signatories to Advanced Nations. 2024. Available online: https://www.researchgate.net/publication/383862496_The_Impact_of_Drones_on_Modern_Warfare_and_Surveillance_Signatories_to_Advanced_Nations (accessed on 12 December 2024).
8. Wang, L.; Zhang, Y.; Wang, Z.; Chen, J.; Yang, L.; Xia, J.; Zhang, Y.; Zhang, J.; Zhu, W.; Zhang, H.; et al. Additive Manufacturing in Construction Using Unmanned Aerial Vehicle: Design, Implementation, and Material Properties. *J. Build. Eng.* **2024**, *98*, 111363. [CrossRef]
9. Jones, R.M. *Mechanics Of Composite Materials*, 2nd ed.; CRC Press: Boca Raton, FL, USA, 2018. [CrossRef]
10. Shahdin, A.; Mezeix, L.; Bouvet, C.; Morlier, J.; Gourinat, Y. Monitoring the effects of impact damages on modal parameters in carbon fiber entangled sandwich beams. *Eng. Struct.* **2009**, *31*, 2833–2841. [CrossRef]
11. Cetrini, A.; Cianetti, F.; Castellani, F.; Astolfi, D. Dynamic Modeling of Wind Turbines. How to Model Flexibility into Multibody Modelling. *Procedia Struct. Integr.* **2018**, *12*, 87–101. [CrossRef]
12. Patil, M.; Cesnik, C.; Hodges, D. Nonlinear Aeroelasticity and Flight Dynamics of High-Altitude Long-Endurance Aircraft. *J. Aircr.* **2001**, *38*, 88–94. [CrossRef]
13. Patil, M.J.; Hodges, D.H.; Cesnik, C.E.S. Limit-Cycle Oscillations in High-Aspect-Ratio Wings. *J. Fluids Struct.* **2001**, *15*, 107–132. [CrossRef]
14. Ahmad, K.; Baig, Y.; Ismail, M. Failure Analysis of High Aspect Ratio Flexible Wing Aeroelastic Loading. *AIP Conf. Proc.* **2018**, *1982*, 020031. [CrossRef]
15. Hodges, D.H.; Pierce, G.A. *Introduction to Structural Dynamics and Aeroelasticity*, 2nd ed.; Cambridge Aerospace Series; Cambridge University Press: Cambridge, UK, 2011. [CrossRef]
16. Li, X.; Wan, Z.; Wang, X.; Yang, C. Aeroelastic Optimization Design of the Global Stiffness for a Joined Wing Aircraft. *Appl. Sci.* **2021**, *11*, 11800. [CrossRef]
17. 2022 Collegiate Design Series SAE Aero Design Rules. Available online: https://saeaerodesign.com/cdsweb/gen/DownloadDocument.aspx?DocumentID=9d92b79f-3da3-404c-946c-327d62a2a5ef (accessed on 10 December 2024).
18. Nettles, A. *Basic Mechanics of Laminated Composite Plates*; NASA Marshall Space Flight Center-RP-1351; NASA: Greenbelt, MD, USA, 1994.
19. Öchsner, A. *Foundations of Classical Laminate Theory*; Springer International Publishing: Cham, Switzerland, 2021. [CrossRef]
20. German, J. *Podstawy Mechaniki Kompozytów Włóknistych*; Politechnika Krakowska: Kraków, Poland, 1996.
21. Gibson, R.F. *Principles of Composite Material Mechanics*, 4th ed.; CRC Press: Boca Raton, FL, USA, 2016. [CrossRef]
22. Chin, A.W.; Truong, S.; Spivey, N. X-56A Structural Dynamics Ground Testing Overview and Lessons Learned. In *AIAA Scitech 2020 Forum*; American Institute of Aeronautics and Astronautics: Orlando, FL, USA, 2020. [CrossRef]
23. Friswell, M.I.; Mottershead, J.E. *Finite Element Model Updating in Structural Dynamics*; Gladwell, G.M.L., Ed.; Solid Mechanics and its Applications; Springer: Dordrecht, The Netherlands, 1995; Volume 38. [CrossRef]
24. Lin, Q.; Yang, C.; Bai, Y.; Qin, J. Structural Strength Analysis and Optimization of Commercial Aircraft Nose Landing Gear under Towing Taxi-Out Conditions Using Finite Element Simulation and Modal Testing. *Aerospace* **2024**, *11*, 414. [CrossRef]
25. Qaumi, T.; Hashemi, S.M. Experimental and Numerical Modal Analysis of a Composite Rocket Structure. *Aerospace* **2023**, *10*, 867. [CrossRef]
26. Giclais, S.; Lubrina, P.; Stephan, C. Aircraft Ground Vibration Testing at ONERA. *Aerosp. Lab* **2016**, *12*, 1–18. [CrossRef]
27. Göge, D.; Böswald, M.; Füllekrug, U.; Lubrina, P. Ground Vibration Testing of Large Aircraft—State-of-the-Art and Future Perspectives. In Proceedings of the 25th International Modal Analysis Conference, Orlando, FL, USA, 19–22 February 2007.
28. Chajec, W. *Aeroelastyczność Samolotów i Szybowców w Praktyce*; Biblioteka Naukowa Instytutu Lotnictwa: Warszawa, Poland, 2022.
29. Box, G.E.P.; Wilson, K.B. On the Experimental Attainment of Optimum Conditions. *J. R. Stat. Soc. Ser. B (Methodol.)* **1951**, *13*, 1–38. [CrossRef]
30. Kleijnen, J.P.C. Response Surface Methodology. In *Handbook of Simulation Optimization*; Fu, M.C., Ed.; Springer: New York, NY, USA, 2015; pp. 81–104. [CrossRef]
31. Carley, K.M.; Kamneva, N.Y.; Reminga, J. Response Surface Methodology. 2004. Available online: http://www.casos.cs.cmu.edu/publications/papers/CMU-ISR-04-136.pdf (accessed on 12 December 2024).
32. Zhao, Q.; Chen, X.; Ma, Z.-D.; Lin, Y. Reliability-Based Topology Optimization Using Stochastic Response Surface Method with Sparse Grid Design. *Math. Probl. Eng.* **2015**, *2015*, 487686. [CrossRef]
33. Smolyak, A.K. Quadrature and Interpolation Formulas for Tensor Products of Certain Classes of Functions. *Sov. Math. Dokl.* **1963**, *4*, 240–243.

34. Clenshaw, C.W.; Curtis, A.R. A Method for Numerical Integration on Automatic Computer. *Numer. Math.* **1960**, *2*, 197–205. [CrossRef]
35. ANSYS Inc. *DesignXplorer User's Guide*; ANSYS Inc.: Canonsburg, PA, USA, 2024.